LEVEL II *F*

ADA081089

CALSPAN ADVANCED TECHNOLOGY CENTER

technical report

DTIC
S ELECTE
FEB 22 1980
D
D

A DIVISION OF CALSPAN CORPORATION

AN A PART COMPANY · P.O. BOX 400 · BUFFALO, NEW YORK 14225

LEVEL

CALSPAN ADVANCED TECHNOLOGY CENTER

(14) CALSPAN-6512-M-1 (A)

(6) DEFORMATION OF THE MARINE INVERSION AND THE DEVELOPMENT OF MARINE FOG AND STRATUS RESULTING FROM WARM WATER PATCHES: NUMERICAL MODELING AND VERIFICATION WITH SATELLITE IMAGERY.

by

(10) C. William Rogers and James T. Hanley

Calspan Report No. 6512-M-1

(15) Contract No. N00014-79-C-0459

November 1979

(9) TECHNICAL REPORT.

(12) 32

DTIC
SELECTED
FEB 22 1980
D

DIVISION OF CALSPAN CORPORATION

410803

79 12 12 013

Table of Contents

LIST OF FIGURES

ACKNOWLEDGMENTS

Section 1

INTRODUCTION AND SUMMARY

Advance warning of marine fog occurrence is an important input to decisions concerning where, when and how naval operations are carried out. Currently, routine operations are hampered by an inability to accurately forecast the location and both temporal and spatial extent of marine fog events, and the fog forecasting problem is being attacked from several approaches. Liepper (1948) and Peterson (1975) use the synoptic model concept in which the evolution of fog is described by stages which are defined by a set of synoptically observable parameters such as inversion height and air and sea surface temperatures. Renard is pursuing fog prediction within the numerical weather prediction framework, and his approach uses multiple discriminant analysis of forecast model outputs and satellite data to identify fog predictors (Van Orman and Renard, 1977 and McNab, 1979). At present, Fleet Numerical Weather Prediction uses the model output statistics procedure in its operational fog forecasting.

A third approach to the forecasting of fog occurrence is through the use of numerical models containing the relevant physics and dynamics of fog formation processes. Before investigation of the application of this approach to forecasting could be successfully undertaken, a better understanding of the physics of marine fog formation was needed.

For the past six years, Calspan has been conducting a field program aboard the NPS ACANIA to investigate fog formation off the California coast. Chief among the results of this study (Pilié et al, 1979) were important correlations of fog and stratus formation with the presence of patches of warm water, low-level mesoscale convergence and unexplained changes in altitude of the marine inversion. A striking similarity (with major scale changes) was recognized between these marine boundary layer phenomena and lake effect winter storm phenomena which previously had been successfully simulated with the Lavoie model (Lavoie 1972) during the Lake Effect Project, headquartered at Calspan (Eadie et al 1971).

1

Consequently, a limited Calspan-sponsored internal research program (Pilié et al, 1978) was conducted in which a modified version of the model was applied to the marine boundary layer problem using idealized meteorological conditions as input. The results indicated that the model could produce inversion height deformations of the right order of magnitude to stimulate stratus and/or fog formation downwind from the warm patches. Under contract No. N00014-79-C-0459 from the Naval Environmental Prediction Research Facility through the Office of Naval Research, the model was then applied to fog/stratus systems occurring off the California coast using actual sea surface temperature patterns, observed winds and inversion height, and satellite-observed cloud fields. This report describes the work done under the latter study.

Specific case studies were selected for which the coastal area was initially clear, but followed by cloud development on the next day. DMSP satellite imagery provided the input sea-surface-temperature pattern on the clear day, and the observed cloud pattern on the following day for model verification. Typical initial conditions included a 700 x 300 km grid, 300 m inversion height and an irregularly shaped warm water patch of approximately 10^4 km^2 area and 2°C warmer than surrounding water.

Results from the model and study of satellite imagery verify earlier conclusions, showing deformation of the inversion and cloud formation above and downwind of the warm water patch. The calculated cloud patterns and locations of maximum cloud liquid water content agree well with observed cloud patterns.

Two important conclusions can be drawn from this research. One is that there is a significant potential for developing a stratus cloud-fog forecasting method based on a suitably modified version of the Lavoie model and using satellite imagery as the basic input. The second is of more immediate value to the Navy. The investigation indicated a very definite correlation between the existence of patches of warm surface water and the downwind formation and development of stratus clouds. Through the stratus lowering process, this correlation should extend also to the downwind presence of fog. It is recommended that the fleet weather service be made aware of this correlation so that it can begin to be incorporated into fog forecast procedures.

Section 2 of this report discusses case selection and analysis procedures, and Section 3 presents the results of individual case studies. Appendix A provides a brief mathematical description of the Lavoie model with emphasis on the treatment of condensation. Conclusions and recommendations based on the results of this effort are presented in Section 4.

Section 2
EXPERIMENTAL DESIGN, CASE SELECTION AND ANALYSIS PROCEDURES

2.1   Lavoie Model

The Lavoie model (Lavoie, 1972) is a two-dimensional representation of the horizontal characteristics of a single-layer air mass capped by an inversion. In its simplest form, it may be described with the aid of Figure 1, which depicts its application to lake-effect snow storms originating over Lake Erie. Input parameters require specification of the surface temperature at each grid point and specification of wind velocity and air temperature entering the experimental region. In the lake effect situation, boundary layer air upwind of the warm lake surface has the same temperature as the cold land surface. The initial inversion height is specified along with a constant potential temperature in the air mass beneath the inversion, the potential temperature at the inversion base, and the potential temperature at the top of the model.

In the version of the Lavoie Model used in this effort, prognostic equations for the horizontal wind components, inversion height, potential temperature, mixing ratio, and cloud liquid water content are included. Evaporation, condensation and latent heat release are also modeled. The spatially uniform upwind boundary conditions are constant during the simulation. Differential heating arising from a non-uniform surface water temperature field produces a perturbation pressure field and an accompanying perturbation wind field. The divergence in this wind field then provides the upward vertical velocity and condensation in the model. With constant upwind boundary conditions and no time variation in the surface temperature field, the model simulations tend toward a steady rate. A mathematical description of the model is presented in Appendix A.

2.2   Case Selection

The model was applied to fog/stratus systems occurring off the California coast. Specific case studies were selected for which the coastal

4

INPUTS

Z — θ_z Potential Temperature at Top of Model

θ_L Potential Temperature at Inversion Base

θ Potential Temperature of Mixed Layer

HI

Altitude

Potential Temperature

INVERSION

LAND TEMPERATURE (COLD)

LAKE TEMPERATURE (WARM)

Wind Velocity In

Wind Velocity Out

(Mass in ≅ Mass out)

Initial Inversion Height
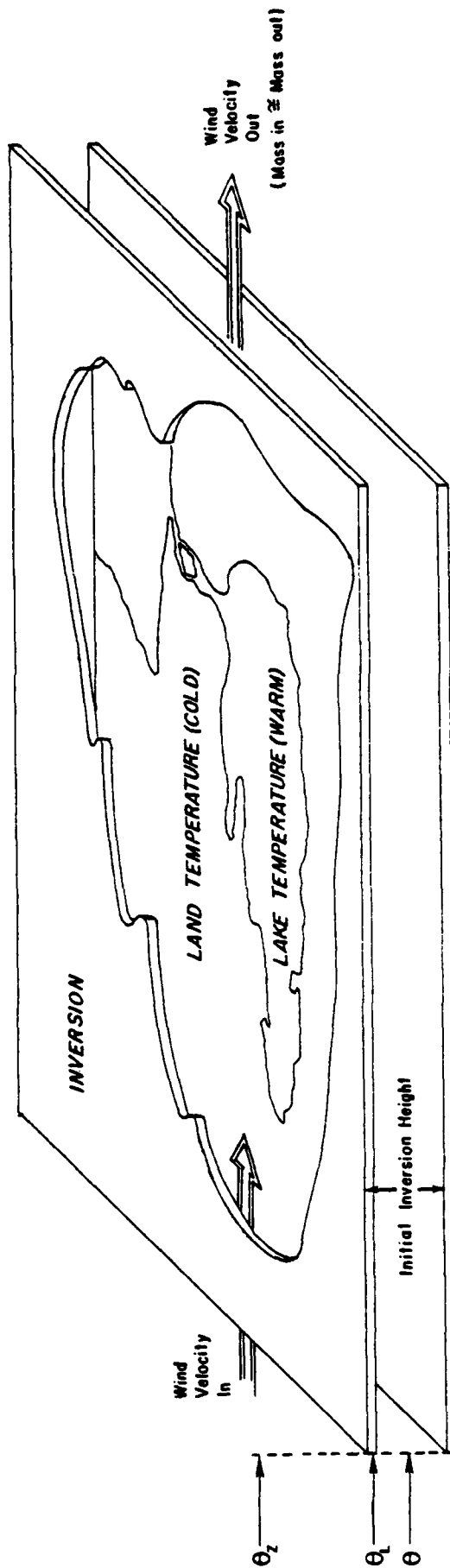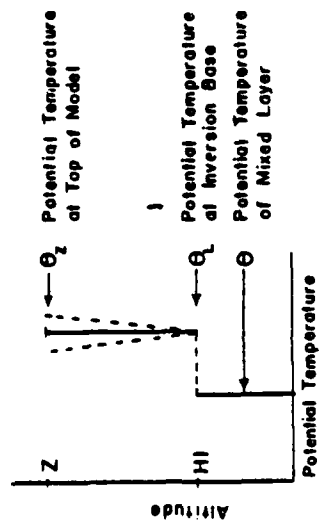
θ_z

θ_L

θ

FIGURE 1: BOUNDARY CONDITIONS FOR THE LAVOIE MODEL

5

area was initially clear, but followed by cloud development on the next day. Satellite IR imagery provided the input sea-surface-temperature pattern on the clear day, and satellite visual imagery of the observed cloud pattern on the following day was used for model verification. Ship reports provided input temperature, humidity, and wind data. Radiosonde data provided the height of the inversion.

A list of potential cases was prepared by examining the NOAA satellite hemispheric imagery contained in the Environmental Satellite Imagery catalogs. A visit was made to the Defense Meteorological Satellite Program Imagery Library located at the University of Wisconsin to find cases for which infrared observations were available on the clear day. The list was reduced to ten possible cases, and the original IR and visible imagery for these cases were returned to Calspan. These cases were further screened to determine those which were fog-stratus cloud systems for which the IR imagery could provide sea surface temperature patterns. Many of the disqualifications arose because the low-resolution IR imagery would not respond to our image enhancement techniques for production of sea surface temperature patterns. High resolution IR imagery would have provided many more usable cases. Of the original ten cases, only two survived for the numerical simulation experiments.

Most of the IR imagery was acquired at low spatial resolution, and the film density variations were weak over the ocean areas. It was necessary to apply image enhancement and processing techniques to these data in order to determine sea surface temperature patterns. Each original transparency was enhanced by copying it onto high contrast film. The transparency was then processed by the Calspan density slicer which provided a false color display of the density variations. (The density slicer system provides for control of both the number of density intervals within a density range and the range of density over which the color display is to occur.) The enhanced negative was input to the system and boundaries of the individual color areas (areas of uniform sea surface temperature) were traced from the color video display. The satellite visual imagery was also analyzed by this system to determine brightness variations within the large scale fog/stratus cloud system.

2.3   Analysis Procedures

A 20 x 20 grid was used in the simulations with a 40 km spacing along one axis and a 20 km spacing along the other axis. Disturbances which are generated by the Lavoie model tend to vary slowly along the wind direction and more rapidly cross wind. The grid, therefore, was designed to provide high spatial resolution in the cross wind direction and lower spatial resolutions along the wind. Since the climatological surface wind direction off the California coast during fog-stratus events is approximately 330°, the larger spaced axis was oriented north-south. (The grid was not oriented along 330° as basic wind flow along a grid axis can produce numerical instability in the simulation.) The warm water area was located near the northwest corner of the grid so that the simulated cloud pattern could extend over the maximum number of grid points. From this grid orientation and location, the warm water patch was specified in grid point space.

Currently, the water temperature field in the model is a patch of water at a uniform temperature surrounded by water at another uniform temperature. For our simulations, the patch is warmer than the surrounding water. Initially, the air temperature equals the cold water temperature so that no heat flows to the air except over the warm water patch.

The warm water patch completely surrounded by cold water was not observed in the cases considered in this study. Instead, peninsular-shaped intrusions of warm water occurred, and for the purposes of modeling these peninsulas were idealized to warm patches. The IR data were analyzed to specify the warm patch independently of the analysis of the observed cloud patterns. Therefore, no bias was introduced toward matching the location of a warm patch to the location of cloud features and vice versa.

In the discussions of the individual cases which follow, the cloud pattern which is used for verification will be presented first in the context of the general synoptic situations. Next, the infrared observations and the definition of the warm patch from them will be discussed. The input to the numerical model including the wind velocity and inversion height will be discussed. Finally, the comparison between the observed and simulated cloud patterns will be made.

Section 3
CASE STUDIES

3.1   Case of 5-6 July 1977

The cloud pattern for this case was observed by the DMSP satellite at 1129 PDT on 6 July 1977 (Figure 2), just west of Monterey Bay. In the spectrum of cloud pattern sizes produced off the California coast, this pattern is small compared to the extensive cloud patterns usually associated with mature fog-stratus systems. From the time sequence of inversion heights at Oakland and Vandenberg AFB, CA, and from the development of a 500 mb ridge and the presence of an extensive stratus-fog system in the DMSP imagery for 7 July, it appears this small cloud area was the beginning development of a more extensive cloud system. Ship observations on 5 May and 6 May indicate that only in this area were the conditions of temperature, dewpoint and inversion height such that cloud could form. Elsewhere, the air was both warmer than the water and dry. The first condition prevents any disturbance formation from heating of the air, and the second condition provides for a lifting condensation level above the low-level inversion.

High resolution infrared observations were available from the DMSP satellite for 0043 PDT, 5 July 1977. Regions of similar grey tone within the original transparency are shown in Figure 3, with hatched areas representing cold temperatures and clear areas representing warm temperatures. The climatological pattern of cold water lying near the coast and warmer water located off shore is evident. Imbedded within this overall pattern are areas of cold and warm water with scales of about 200 km. The elongated warm area, A, located west and northwest of Monterey Bay was the warm water patch for this case. This patch is bounded on the east by a cold water eddy which protrudes westward from north of Monterey Bay. Such westward protrusions of cold water are common in this region, so that the area west of Monterey Bay appears to be a favored location for development of warm water patches.
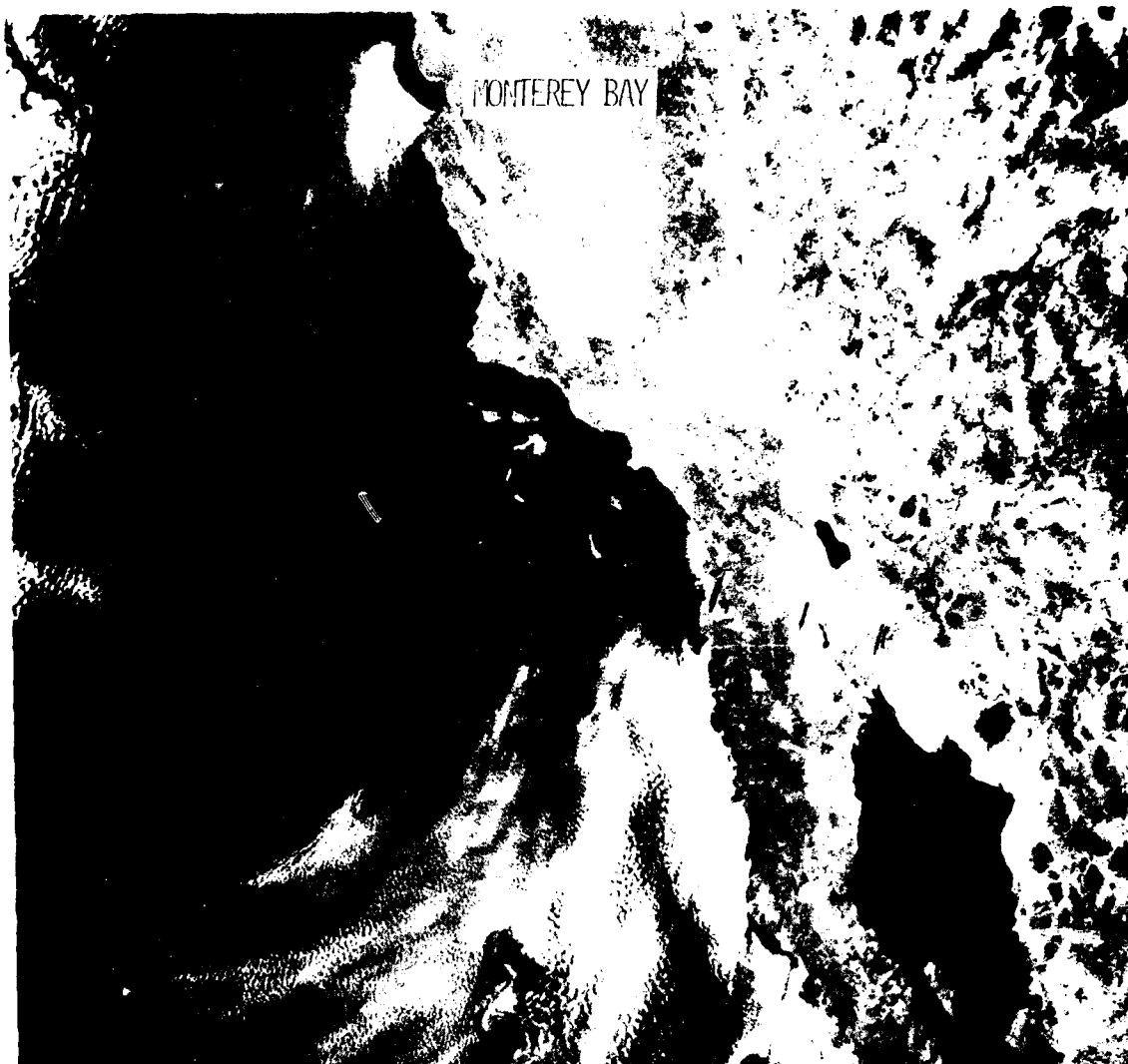
FIGURE 2: DMSP VISUAL IMAGE OF SOUTHERN CALIFORNIA, 1129 PDT 6 JULY 1977

14.0   12.3   11.2

11.3

13.3

12.0

17.3

10.6

A   10.6   12.8   MONTEREY BAY

14.5

12.2

15.0

POINT CONCEPTION

0   50   100   150   200   KM
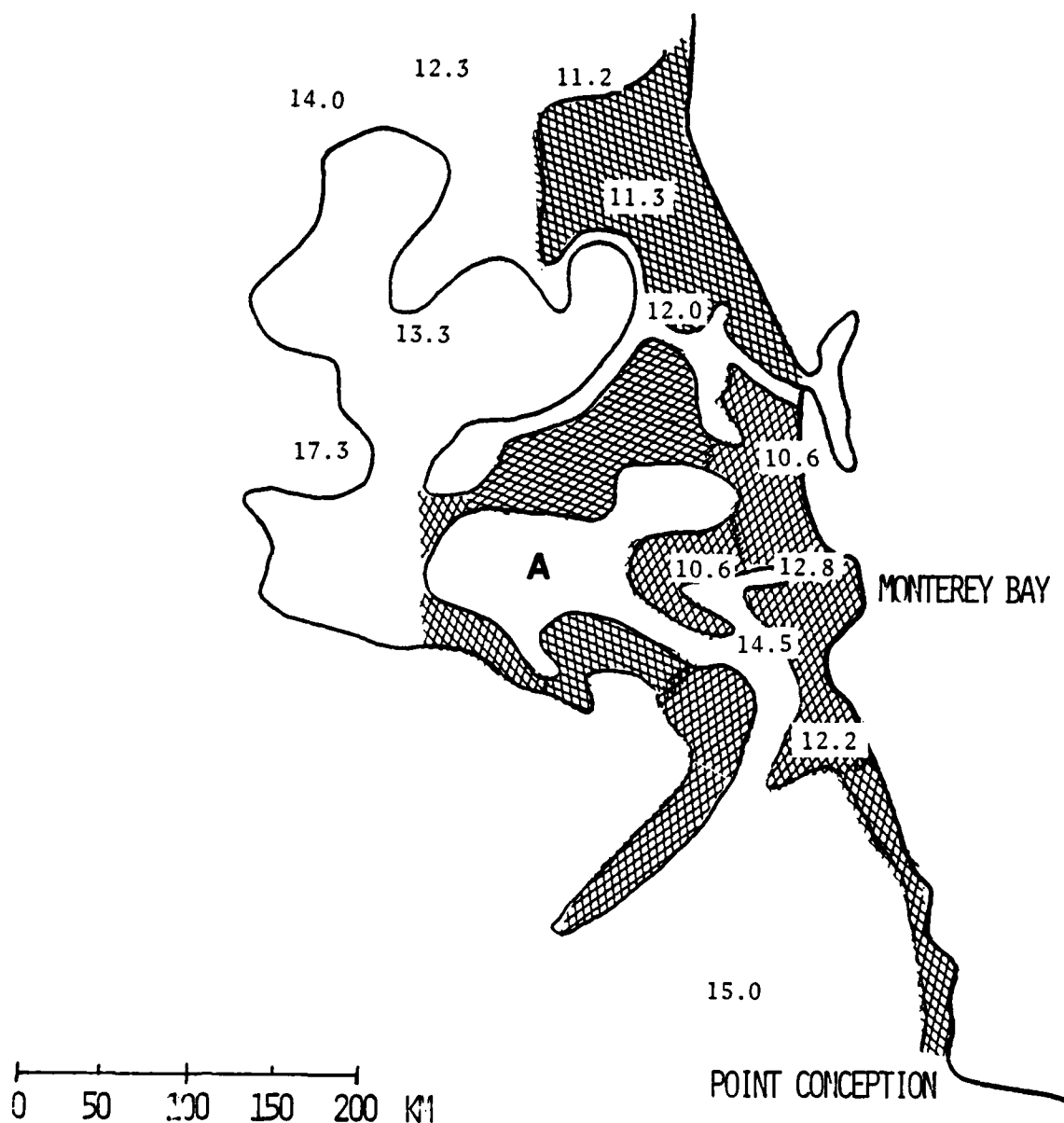
CROSSHATCHED AREAS ARE COLD WATER
BLANK AREAS ARE WARM WATER
NUMBERS ARE SHIP OBSERVATIONS OF SEA SURFACE TEMPERATURE FOR THE
PERIOD, 5-7 JULY 1977

FIGURE 3:   SEA SURFACE TEMPERATURE PATTERN DERIVED FROM DMSP IR IMAGE,
0043 PDT 5 JULY 1977

For input into the Lavoie model simulation, the temperatures of the warm patch and the surrounding cold water were needed. All available ship reports for the period 5-7 July 1977 were used to obtain the sea surface temperatures shown in Figure 3. These data were supplied by Professor R. Renard of NPS, technical monitor for this contract, from a National Climatic Center data tape of ship observations. The data indicate that the warm patch temperature was ∿14°C while the surrounding colder water was ∿12°C.

Ship reports indicated that wind was 310° at 10 m sec^{-1}, air temperature was near 12°C, and the dewpoint spread was 3°C. Vertical temperature soundings from Oakland, CA, and Vandenberg AFB, CA, indicated that the base of the inversion was at 300 m.

A model simulation was run using the above parameter values as initial and upwind boundary conditions. The simulation was run out to six hours which allowed steady state conditions to develop in the cloud region downwind of the warm patch.

In Figure 4, the cross hatched area is the warm patch as depicted in grid point space, the bold arrow represents the direction of the initial, undisturbed wind, the solid lines are isopleths of the cloud liquid water as simulated by the model, and the dashed lines are the observed cloud pattern. The observed cloud pattern representation was obtained by subjectively outlining cloud field features as seen in the film transparency. The isopleth labeled (1) outlines the outer edge of the faintest cloud discernible in the film, and the isopleth labeled (2) outlines the area of overcast cloud. The line labeled (3) delineates a bright cloud core located within the region of overcast cloud.

In comparing model simulations with observed cloud fields, the absolute values of cloud liquid water should not be considered. Rather, with the crude parameterization of condensation used in the model, comparisons are much more appropriate between the major characteristics of the simulated and observed cloud patterns, such as orientation of major cloud axis, location of the center of the thickest (brightest) cloud, and location of gradients of cloud intensity.

310 @ 10 M/S

MONTEREY BAY

POINT CONCEPTION

2

3

0.7

0.5

1

0.1

0   50   100   150   200   KM

—— SIMULATED LIQUID WATER CONTENT (G/M^3)

——— OBSERVED CLOUD PATTERN
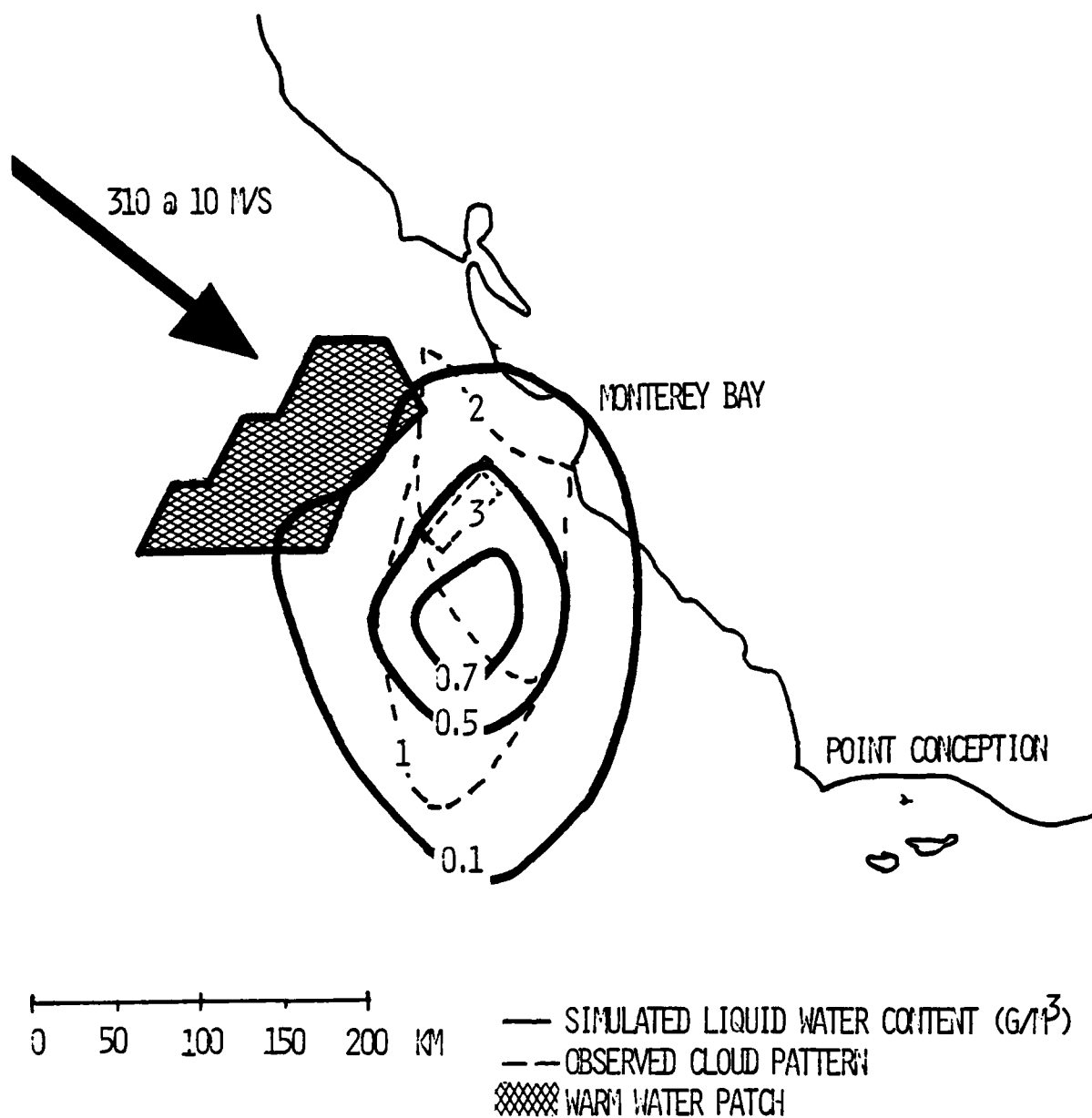
▨▨▨ WARM WATER PATCH

FIGURE 4:   SIMULATED AND OBSERVED CLOUD PATTERNS, 5-6 JULY 1977

The correspondence between the general orientation and shape of the simulated and observed cloud patterns (Figure 4) is remarkable. The 0.1 isopleth of liquid water content readily outlines the observed cloud, while the central isopleths of the LWC are elongated north-south similar to the observed cloud pattern. The area of maximum LWC is somewhat larger and located slightly downwind of the bright core of the observed cloud.

3.2 Case of 7-8 June 1978

For this case, the cloud pattern along the California coast was more typical of the widespread fog/stratus systems. The pattern was narrow (100 km wide) at its northern end near Cape Mendocino and wide (650 km) in its southern portion near San Diego as shown in the DMSP visual observation taken at 1209 PDT on 8 June 1978 (Figure 5). Synoptically, this period was characterized by a ridge at 500 mb and at the surface by the typical thermal low over California coupled with offshore high pressure producing northwesterly flow in the coastal regions.

These widespread fog/stratus systems owe their existence and characteristics to many processes which span the spectrum of meteorological scales, from the micro- through the meso- to the synoptic. The size and location of the overall cloud pattern is controlled by synoptic scale processes such as those which change the inversion height and the marine boundary-layer flow around the subtropical high. The Lavoie model is designed to simulate processes of mesoscale dimensions and, therefore, cannot be expected to reproduce the overall dimensions and characteristics of fog/stratus cloud system.

The mesoscale cloud patterns which the model does produce can be thought of as perturbations superposed on the synoptic scale cloud field by the underlying warm water patches. When the warm patch is imbedded in the large-scale fog/stratus system, the resulting perturbations may produce any or all of the following:

1. thicker cloud due to an increase in height of the marine inversion or a lowering of the lifting condensation level.

13

FIGURE 5: DMSP VISUAL IMAGE OF WEST COAST OF U.S. AND EASTERN PACIFIC,
1209 PDT 8 JUNE 1978

2.   larger liquid water from either or both increased evaporation over the warm patch and increased condensation in the regions of mesoscale updrafts.

3.   regions with higher density of cumulus clouds because of the additional moisture and presence of updrafts.

Because the DMSP visual resolution is ∿2 nmi, all these processes (in particular No. 3) may tend to produce larger integrated liquid water contents and hence brighter areas within the overall cloud pattern. Therefore, in the discussions which follow, we compare variations in brightness in the observed cloud field with variations in the cloud simulated liquid water content.

Low resolution DMSP IR data at 1226 PDT on 7 June 1978 were processed by the Calspan density slicer system, and the corresponding density isopleths are shown in Figure 6. Again in the figure, cold water regions are hatched and warm water areas are blank. As in the previous case, cold water was observed along the coast, and the water temperature in general increased with distance from the coast. Within this overall trend, areas of warm water were observed embedded in the cold water. In this case, there are two such warm patches; Area A was located just west of Monterey Bay in the region where one was observed in the previously described situation of 5-7 July 1977. A second and larger warm water patch, Area B, was located northwest of Point Conception.

For this case, ship reports were obtained from archival data tapes at Fleet Numerical Weather Facility in Monterey. The reports were very scarce, and sea surface temperatures of the warm patches could not be determined from these data. Discussions with Dr. C. Mooers of the NPS and Mr. L. Breaker of NOAA/NESS Redwood City, California, who are studying these warm patches and vortices, indicate that the 2°C temperature difference found in the previous case is probably typical. That value was used in the simulation.

The available ship reports did suggest that the surface meteorological conditions, except for a wind direction of 330° near Area A and a wind direction of 310° near Area B, were the same as in the previously discussed case. Vertical temperature soundings for Vandenberg and Oakland again indicated a 300 m inversion height.

MONTEREY BAY

POINT CONCEPTION

| 0 | 50 | 100 | 150 | 200 | KM |

CROSSHATCHED AREAS ARE COLD WATER
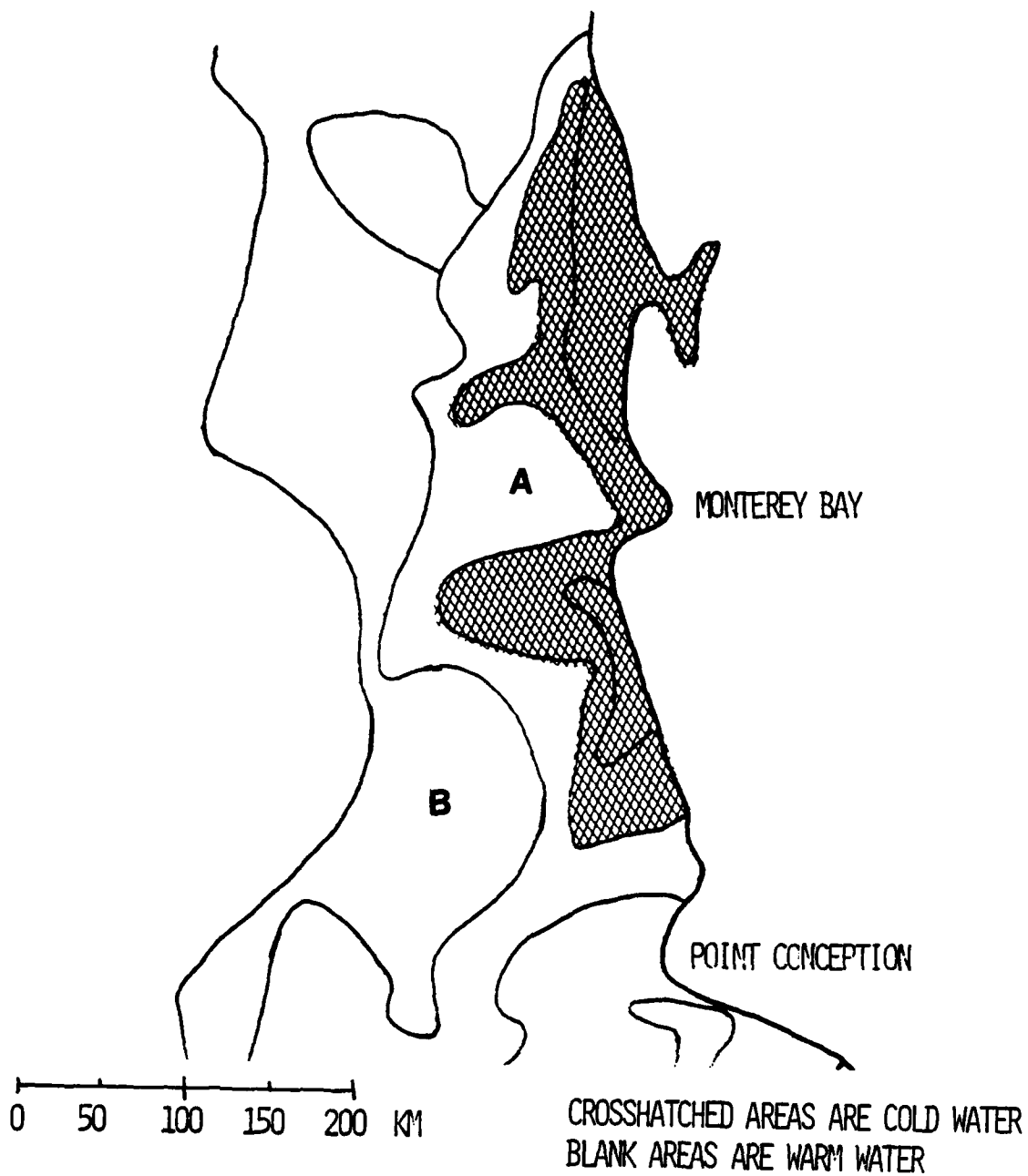BLANK AREAS ARE WARM WATER

FIGURE 6:   SEA SURFACE TEMPERATURE PATTERN DERIVED FROM DMSP IR IMAGE,
1226 PDT 7 JUNE 1978

The model simulation was run using the above parameter values as initial and upwind boundary conditions. The simulation was run out to 12 hours which allowed steady state conditions to develop in the cloud region downwind of the warm patch.

3.2.1   Warm Patch "A"

Figure 7 shows the simulated and observed cloud patterns. In this case the isopleths of observed cloud brightness were obtained by analyzing the visual imagery with the density slicer. The correspondence between the simulated and observed cloud pattern is again striking, with the north-south elongation of both sets of isopleths. In particular, note the location of both the maximum in LWC and the brightest core of the observed cloud pattern (Isopleth #3) downwind from the warm patch, with the cross wind dimensions being equal to or less than that of the warm patch. Also, notice the correspondence between the gradients in the two sets of isopleths on the ocean side of the observed bright core.

3.2.2   Warm Patch "B"

Figure 8 shows the observed and simulated cloud patterns for warm patch "B" located west and northwest of Point Conception. The wind direction used in this case was 310°; the other input parameters had the same values as those used in the simulation for warm patch "A".

Again, the general north-south elongation of observed cloud is reproduced by the simulated cloud pattern. In particular, the bright core in the observed cloud pattern is well-delineated in its central portion by the isopleth of maximum liquid water content. However, in this southern portion of the large scale fog-stratus pattern, the western edge of the simulated cloud is located east of western edge of the observed cloud. This discrepancy is not surprising since at this southern latitude the location of the western edge of the observed cloud is controlled by factors other than flow
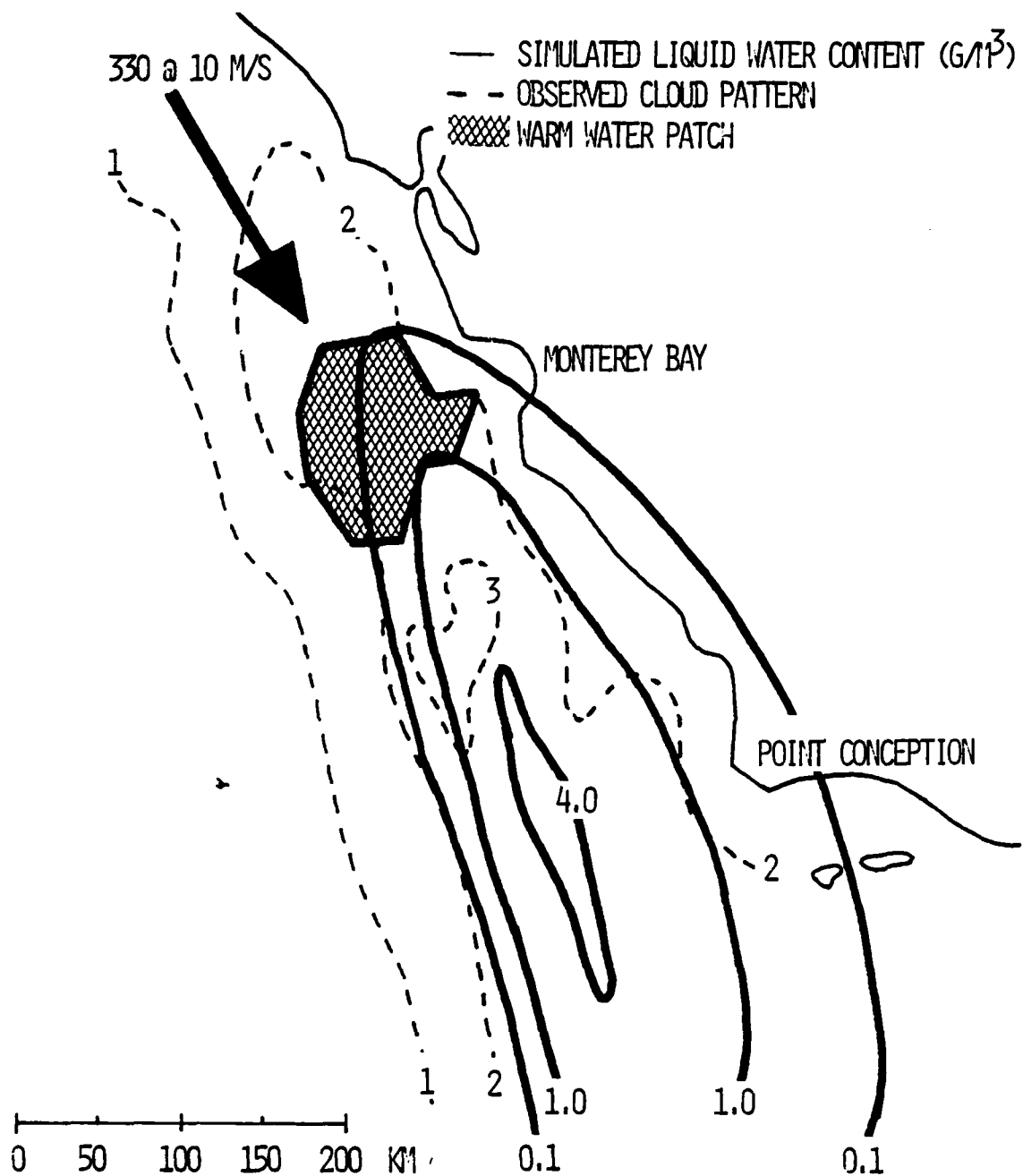
FIGURE 7: SIMULATED AND OBSERVED CLOUD PATTERNS, WARM PATCH "A",
7-8 JUNE 1978

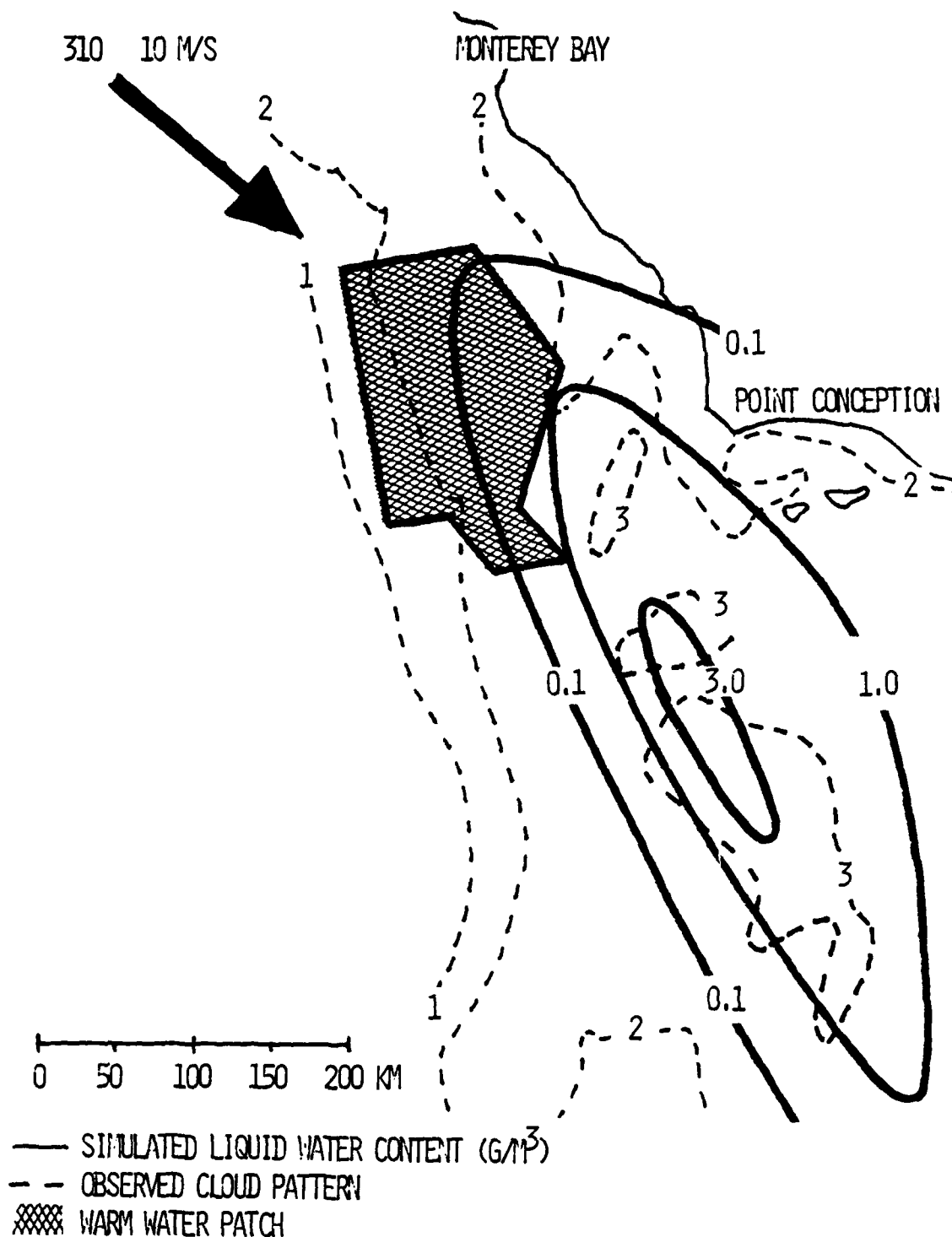18

FIGURE 8: SIMULATED AND OBSERVED CLOUD PATTERNS, WARM PATCH "B", 7-8 JUNE 1978

310   10 M/S

MONTEREY BAY

POINT CONCEPTION

——— SIMULATED LIQUID WATER CONTENT (G/M³)
– – OBSERVED CLOUD PATTERN
▨ WARM WATER PATCH

0   50   100   150   200 KM

over warm water patches, which is what the model simulates. For example, the location of the western cloud edge could result from advection of cloud by the marine boundary layer flow. In this particular case, the wind direction probably turns to the north and northeast as the air flows around the eastern end of the sub-tropical high.

Section 4

CONCLUSIONS AND RECOMMENDATIONS

The results presented here represent the initial application of a numerical model, designed originally to study snow storms occurring downwind of a warm lake, to stratus/fog systems occurring downwind of the warm water patches in the ocean. Major differences between the two applications include: 1.) an order of magnitude difference in inversion height, with the base of the marine layer inversion being typically a few hundred meters above the surface; and 2.) air-water temperature differences of a couple of degrees centigrade over the ocean compared to 5-15°C over the lake.

Using observed sea surface temperature patterns and meteorological conditions as input, Lavoie model simulations reproduce quite well the location and orientation of the major axis of the cloud field and predict a maximum in liquid water content near the bright core of the observed cloud. The location of the seaward edge of the cloud pattern is reproduced but with somewhat less skill than for the other cloud field features.

This limited feasibility study has demonstrated that a significant potential exists for developing a stratus cloud-fog forecasting method based on a suitably modified version of the Lavoie model which uses satellite imagery as the basic input. To realize this potential, additional work is required to examine the sensitivity of model simulations to variations in input parameters such as inversion height and wind velocity. In addition, the areal coverage provided by the numerical grid must be expanded in order to encompass entire fog/stratus systems. Further, satellite imagery shows that frequently more than one warm water patch exists within the larger areas of fog/stratus systems; the numerical model must be modified to handle more realistic sea surface temperature patterns, including multiple warm water patches.

Further, the study has demonstrated through the use of routinely available satellite imagery that marine stratus/fog cloud fields, and in particular, bright core areas, are located downwind of warm water patches. Through the stratus lowering process, this correlation should extend also to the downwind presence of fog. This conclusion is of immediate value to the Navy, and it is recommended that the fleet weather service be made aware of

21

this correlation so that it can be immediately incorporated into fog forecast procedures. However, ground truth data are needed to more fully develop and quantify the correlation between the observed bright core areas in the stratus cloud and surface weather conditions.

REFERENCES

1. Eadie, W.J., U. Katz and C.W. Rogers, 1971: Investigations of Lake-Effect Snowstorms, Final Report on Contract No. E22-59-71(N), 29 November 1971. CAL Report No. VC-3034-M-1, Cornell Aeronautical Laboratory, Inc., Buffalo, NY.

2. Lavoie, R.L., 1972: A Mesoscale Numerical Model of Lake Effect Storms, J. Atmos. Sci., 29, 1025-1040.

3. Leipper, D.F., 1948: Fog Development at San Diego, California, J. Mar. Res., 7, 337-346.

4. McNab, O.F., 1979: Analysis of Statistical Parameters Derived from Satellite Digital Data (July 1968 GOES-West) for Use in Diagnosing Marine Fog Areas. M.S. Thesis, Department of Meteorology, Naval Postgraduate School, Monterey, California, 68 pp.

5. Peterson, C.A., 1975: Fog Sequences on the Central California Coast with Examples. M.S. Thesis, Department of Meteorology, Naval Postgraduate School, Monterey, CA.

6. Pilié, R.J., C.W. Rogers, and J.T. Hanley, 1978: Application of the Lavoie Model Within the Unstable Marine Boundary Layer. Calspan Report No. 85-416. Calspan Corporation, Buffalo, NY 14225.

7. Pilié, R.J., E.J. Mack, C.W. Rogers, U. Katz and W.C. Kocmond, 1979: The Formation of Marine Fog and the Development of Fog-Stratus Systems Along the California Coast, J. Appl. Met., 18, 1275-1286.

8. VanOrman, B.L., 1977: Statistical Diagnostic Modeling of Marine Fog Using Model Output Parameters. M.S. Thesis, Department of Meteorology, Naval Postgraduate School, Monterey, CA.

APPENDIX A

LAVOIE MODEL

Mathematically, the model has the form shown in Figure A-1. Initially the advection term equals zero in equation 1 and the Coriolis and frictional terms are specified by the initial velocity field. The large scale pressure force and thermal wind in the upper layer are selected to balance the latter two terms. The direct surface heating, computed from equation 3, stimulates localized pressure changes which produce accelerations (equation 1) and a non-zero divergence field. The last term in equation 4 is the vertical velocity at the inversion base, determined by the product of inversion height and divergence. This term causes a change in the inversion height and extends the pressure perturbation by altering the fraction of air beneath and above the inversion in the model. The inversion height deformation term is included in subsequent computations of acceleration in equation 1.

Introduction of Moisture

The prognostic equation for average water vapor content in the well-mixed layer which has been incorporated into the Lavoie model takes the form

$$\frac{\partial r}{\partial t} = -\vec{V} \cdot \nabla r + EVAP - \frac{COND}{\bar{\rho} H} \tag{5}$$

where r is the average mixing ratio for the layer, $\vec{V}$ is the horizontal wind vector, H is the height of the capping inversion surface or the thickness of the layer, and COND is the net condensation rate in a unit column of the layer of mean density $\bar{\rho}$. EVAP is a parameterization of evaporation from the water surface by the bulk aerodynamic method and is given by

$$EVAP = \frac{C_E \left| \vec{V} \right| (r_s - r)}{H} \tag{6}$$

where the surface mixing ratio r_s is assumed equal to the saturation mixing ratio at the ocean surface temperature, and C_E is a drag coefficient for evaporation assumed equal to a drag coefficient for exchange over the ocean.

ADVECTIVE TERM   CORIOLIS TERM   FRICTIONAL FORCE   LARGE SCALE PRESSURE FORCE

$$\frac{\partial u}{\partial t} = -\vec{V}\cdot\nabla u + fv - C_{DRAG}|\vec{V}|u - \frac{1}{\rho}\frac{\partial P}{\partial x}$$

PERTURBATION PRESSURE FORCES

INVERSION HEIGHT DEFORMATION   SURFACE HEATING

$$+ \frac{g}{\theta_L}\left[\theta - \frac{\theta_L+\theta_z}{2}\right]\frac{\partial H}{\partial x} + \frac{gH}{2\theta}\frac{\partial \theta}{\partial x} \qquad (1)$$

$$\frac{\partial v}{\partial t} = \text{SIMILAR TO } \frac{\partial u}{\partial t} \qquad (2)$$

ADVECTIVE TERM   SURFACE HEATING

$$\frac{\partial \theta}{\partial t} = -\vec{V}\cdot\nabla\theta + C_{HEAT}|\vec{V}|(\theta_{SURFACE} - \theta) \qquad (3)$$

ADVECTIVE TERM   VERTICAL VELOCITY (DIVERGENCE) TERM

$$\frac{\partial H}{\partial t} = -\vec{V}\cdot\nabla H - H\left(\frac{\partial u}{\partial x} + \frac{\partial v}{\partial y}\right) \qquad (4)$$

FIGURE A-1: MATHEMATICAL FORM OF LAVOIE MODEL

The prognostic equation for the total mass of cloud water Q in a unit column of the layer is written

$$\frac{\partial Q}{\partial t} = \vec{V} \cdot \nabla Q + COND \tag{7}$$

In addition, the potential temperature equation of the model was modified by addition of a term accounting for the release of latent heat of condensation. The potential temperature equation becomes

$$\frac{\partial \theta}{\partial t} = -\vec{V} \cdot \nabla \theta + \frac{C_H |\vec{V}| (\theta_s - \theta)}{H} + \frac{L}{C_p} COND \tag{8}$$

where θ_s is the surface temperature, C_H is a drag coefficient for heat exchange, L is the latent heat of condensation, and C_p is specific heat of air at constant pressure.

The condensation rate in a unit column of the layer can be computed by assuming that liquid water is generated by the mesoscale updrafts in a moist adiabatic process taking place between cloud base and the mean cloud tops at the capping inversion surface. This can be expressed mathematically as

$$COND = -\bar{\rho} \int_C^H \frac{dr_s}{dt} \, W \, dZ \tag{9}$$

where $\frac{dr_s}{dt}$ is the derivative of saturation mixing ratio r_s with height Z, $W = -Z\nabla \cdot \vec{V}$ is the mesoscale vertical velocity predicted by the model, and C is the cloud base height or lifting condensation level computed from r and θ. If we now simplify the integral by assuming an appropriate mean value for $\frac{dr_s}{dt}$, we obtain

$$
\begin{aligned}
COND &= \bar{\rho} \, \overline{\frac{dr_s}{dt}} \, \nabla \cdot \vec{V} \int_C^H Z \, dZ \\
&= \bar{\rho} \, \overline{\frac{dr_s}{dt}} \, \nabla \cdot \vec{V} \left(\frac{H^2 - C^2}{2} \right) \\
&= -\bar{\rho} \, \overline{\frac{dr_s}{dt}} \, W_H \left(\frac{H^2 - C^2}{2H} \right)
\end{aligned} \tag{10}
$$

where $W_H = -H\nabla \cdot \vec{V}$ is the vertical velocity at the inversion surface H .

26

This computational procedure for condensation produced very small
maximum values of cloud liquid water, of the order of 0.05 g/m^3. From our
observations of marine fogs, we know that LWC should be at least 0.10 g/m^3
for young fogs and greater than that for stratus clouds. Therefore, a
parameterization of condensation which had been used in application
of the Lavoie model to lake effect snow storms to increase the condensation
was used. This formulation was

$$COND = - \rho r W_H.$$ (11)

Comparison of (11) to (10) shows that the two are dimensionally equivalent. The
values of cloud LWC computed from this formulation were too large. They could
be realistically reduced by multiplying the right-hand side of (11) by some height
factor similar to that contained in (10) which would represent a fraction of
the layer which is occupied by cloud.